Solution Structure of the Human CC Chemokine 2: A Monomeric Representative of the CC Chemokine Subtype[†,‡]

Heinrich Sticht,[*,§] Sylvia E. Escher,[||] Kristian Schweimer,[§] Wolf-Georg Forssmann,[||] Paul Rösch,[§] and Knut Adermann[||]

Lehrstuhl für Biopolymere, Universität Bayreuth, D-95440 Bayreuth, Germany, and Niedersächsisches Institut für Peptid-Forschung (IPF), D-30625 Hannover, Germany

Received January 11, 1999; Revised Manuscript Received March 11, 1999

ABSTRACT: HCC-2, a 66-amino acid residue human CC chemokine, was reported to induce chemotaxis on monocytes, T-lymphocytes, and eosinophils. The three-dimensional structure of HCC-2 has been determined by ^{1}H nuclear magnetic resonance (NMR) spectroscopy and restrained molecular dynamics calculations on the basis of 871 experimental restraints. The structure is well-defined, exhibiting average root-mean-square deviations of 0.58 and 0.96 Å for the backbone heavy atoms and all heavy atoms of residues 5−63, respectively. In contrast to most other chemokines, subtle structural differences impede dimer formation of HCC-2 in a concentration range of 0.1 μM to 2 mM. HCC-2, however, exhibits the same structural elements as the other chemokines, i.e., a triple-stranded antiparallel β-sheet covered by an α-helix, showing that the chemokine fold is not influenced by quaternary interactions. Structural investigations with a HCC-2 mutant prove that a third additional disulfide bond present in wild-type HCC-2 is not necessary for maintaining the relative orientation of the helix and the β-sheet.

HCC-2[1] is a member of the chemokine protein family, a group of small proinflammatory cytokines (8−10 kDa) that are involved in the selective recruitment of a large variety of leukocytes as well as in their activation (*1*, *2*). Two main subfamilies, CXC and CC chemokines, are distinguished by the relative position of the first two of four conserved cysteines. Those are either separated by one amino acid or directly adjacent to each other (*3*). CC chemokines stimulate monocytes, T-lymphocytes, basophiles, and eosinphiles, whereas CXC chemokines, like interleukin-8, act predominantly on neutrophiles (*4*, *5*). All chemokines signal through G-protein-coupled seven-transmembrane receptors (*6*).

Recently, the gene of HCC-2 was identified on chromosome 17 and expression analysis showed not only its regular monocistronic but also a bicistronic transcript of the adjacently localized gene for HCC-1 (*7*). It encodes a 113-amino acid protein containing a putative 21-residue signal peptide and the mature 92-amino acid HCC-2 protein. Unexpectedly, recombinant expression of HCC-2 resulted in different NH_2-terminally truncated forms of HCC-2 depending on the expressing system. In *Pichia pastoris*, HCC-2 containing 66 amino acids corresponding to sequence positions 48−113 was obtained (*7*), whereas expression in *Escherichia coli* resulted in HCC-2 containing 68 residues (positions 46−113) and the putative mature wild-type HCC-2 (22−113) containing 92 residues (*8*). These variants were shown to induce chemotaxis on human monocytes, T-lymphocytes, and, to a lesser degree, in eosinophils (*7*−*9*). It was demonstrated that the effects of HCC-2 are mediated through the CCR-1 and CCR-3 receptors (*7*−*9*).

To understand the complex interplay between chemokines and their receptors on a structural basis, several three-dimensional chemokine structures have been determined by either NMR spectroscopy or X-ray crystallography: PF-4 (*10*, *11*), IL-8 (*12*, *13*), MGSA (*14*−*16*), Chi1 (*17*), CINC/Gro (*18*, *19*), NAP-2 (*20*), MIP-2 (*21*), SDF-1α (*22*), MIP-1β (*23*), RANTES (*24*, *25*), MCP-1 (*26*, *27*), MCP-3 (*28*, *29*), and Eotaxin (*30*). In all cases, the monomeric subunit exhibits a quite similar secondary and tertiary structure consisting of a triple-stranded antiparallel β-sheet packed against a carboxy-terminal α-helix, while the quaternary contacts of these proteins vary strongly. For the members of the CXC family, two monomers associate to form an extended six-stranded β-sheet with most of the subunit−subunit interactions formed between the first β-strand of each

[†] This work was supported in part by a grant from Bundesministerium für Bildung, Wissenschaft, Forschung und Technologie (to K.A., FKZ 0311815). S.E.E. is a scholar of the Fonds der Chemischen Industrie.

[‡] The coordinates have been deposited in the Brookhaven Protein Data Bank (file name 2HCC).

* To whom correspondence should be addressed. Phone: +49 921 553542. Fax: +49 921 553544. E-mail: Heinrich.Sticht@Uni-Bayreuth.de.

[§] Universität Bayreuth.

[||] Niedersächsisches Institut für Peptid-Forschung (IPF).

[1] Abbreviations: CCR-1, chemokine receptor-1; Chi1, chimeric chemokine of IL-8 (residues 1−53) and MGSA (residues 54−72); CINC, cytokine-induced neutrophil chemoattractant; COSY, correlated spectroscopy; DIEA, *N*,*N*-diisopropylethylamine; DQF-COSY, double-quantum-filtered COSY; ESMS, electrospray mass spectrometry; Fmoc, fluorenylmethoxycarbonyl; HBTU, 2-(1*H*-benzotriazol-1-yl)-1,1,3,3-tetramethyluronium hexafluorophosphate; HCC-2, human CC chemokine 2; HPLC, high-performance liquid chromatography; IL-8, interleukin-8; MCP, monocyte chemoattractant protein; MGSA, melanoma growth stimulatory activity; MIP, macrophage inflammatory protein; NAP-2, neutrophil activating protein-2; NMR, nuclear magnetic resonance; NOE, nuclear Overhauser effect; PF-4, platelet factor 4; RANTES, regulated on activation, normal T-cell expressed, and secreted; rmsd, root-mean-square deviation; SDF-1α, stromal cell-derived factor 1α; TOCSY, total correlation spectroscopy; TPPI, time-proportional phase incrementation.

10.1021/bi990065i CCC: $18.00
Published on Web 04/24/1999

monomer. Generally, a dimeric structure is observed for all of these chemokines, while PF-4 and NAP-2 form tetramers which contain two IL-8-like dimers being packed back to back. Among CC chemokines MIP-1β, RANTES, and MCP-1, a completely different quaternary arrangement was observed in which the dimer interface is mainly formed by residues of the extended amino terminus. This different type of subunit arrangement results in an elongated, cylindrical dimer, which is contrast to the globular dimers formed by the CXC chemokines. For CC chemokine MCP-3, both a dimerization mode similar to that of CXC chemokines (*29*) and a monomeric form (*28*) have been reported, and for eotaxin, a monomer−dimer equilibrium was observed under a wide range of conditions (*30*).

The relevance of dimerization for biological activity, however, was one of the more controversial issues concerning chemokines, with contradictory reports implicating either the dimer or the monomer of the chemokine as the biologically active form (*31*−*33*). An extensive study suggested that most chemokines are monomeric at physiological concentrations, suggesting that dimerization purely is a structural phenomenon observed at high concentrations but has no functional role (*34*). Therefore, one goal of structural studies is the investigation of chemokines which are monomeric at millimolar concentrations, thus allowing structure determination in the absence of quaternary interactions and the identification of those structural elements required for receptor interaction. HCC-2 appears to be a promising target for such studies, since its shorter amino terminus makes the formation of dimers less likely than in other chemokines.

One additional unusual structural property of HCC-2 is the presence of two additional cysteine residues forming a third disulfide bond. Among the CC chemokines, six cysteines were only found for human Ckβ8 and some murine homologues (*35*). Until now, no three-dimensional structure has been available for one of these triple disulfide-bonded chemokines; thus, nothing is known about the influence of the third disulfide bond on the secondary and tertiary structure as well as on the mode of oligomerization.

MATERIALS AND METHODS

Protein Expression and Peptide Synthesis. The 66-residue wild-type (wt) HCC-2 that corresponds to residues 48−113 of the HCC-2 precursor protein was expressed in *P. pastoris*, purified, and characterized as described previously (*7*). [Ala^{17,57}]HCC-2 was synthesized on a 433A peptide synthesizer (Perkin-Elmer) by Fmoc chemistry and activation in the presence of HBTU/DIEA on a preloaded TentaGel S PHB-Ile(Fmoc) resin. Side chain protection of N^{α}-Fmoc amino acids was as follows: Arg(Pbf), Asp(OtBu), Glu(OtBu), Gln(Trt), Lys(Boc), Ser(tBu), Thr(tBu), and Tyr(tBu). Each coupling cycle was terminated by a capping step with acetic anhydride. The two disulfide bonds of the peptide were selectively introduced using trityl protection for Cys7 and Cys46 and acetamidomethyl protection for Cys6 and Cys30. Subsequent steps of oxidation by air and iodine were employed. The crude peptide was purified by C18 HPLC; its identity and purity were checked by capillary zone electrophoresis, analytical C18 HPLC, ESMS analysis, and Edman degradation. The synthesis of this chemokine will be described in detail elsewhere.

Size-Exclusion Chromatography. HCC-2 was loaded at a concentration of 0.2−1 μg/mL on a Superdex 75 column (Pharmacia) equilibrated with 100 mM Na_2SO_4 containing 50 mM K_2HPO_4 (pH 7) with a flow rate of 0.5 mL/min (UV detection at 214 nm). The column was calibrated with a reference mixture containing bovine serum albumin (67 kDa), ovalbumin (43 kDa), chymotrypsin A (25 kDa), ribonuclease A (13.7 kDa), and ubiquitin (8.5 kDa).

NMR Spectroscopy. Sample concentrations used for NMR spectroscopy were 1.7 mM for wt-HCC-2 and 1.3 mM for [Ala^{17,57}]HCC-2 in 0.5 mL of H_2O/D_2O [9:1 (v/v), pH 3.0] or D_2O (99.99 at. %). Homonuclear two-dimensional experiments were performed in H_2O/D_2O at 298 K on a Bruker DRX600 spectrometer equipped with a triple-axis gradient probe head. A clean TOCSY experiment with an 80 ms mixing time using the DIPSI2rc mixing sequence (*36*) and a double-quantum filtered COSY spectrum were recorded. NOESY spectra were recorded with 120 and 200 ms mixing times. All spectra were measured in the phase-sensitive mode using the States−TPPI method (*37*). Water suppression in the TOCSY and NOESY experiments was achieved by "excitation sculpting" (*38*). In the COSY experiment, the water resonance was suppressed by coherence selection with magic angle gradients (*39*). Experiments in D_2O were acquired on a Bruker AMX400 spectrometer. Slowly exchanging amide protons were identified from a series of short (approximately 4 h) TOCSY spectra collected immediately after redissolving the lyophilized sample in D_2O. Additionally, a NOESY spectrum (80 ms mixing time) and a COSY spectrum with a flip angle of 45° were recorded. The residual HDO signal was suppressed using presaturation. All data sets were recorded with an 11 ppm sweep width and contained 2K (F_2) and 256−512 (F_1) complex data points. Prior to Fourier transformation, the time domain signals were multiplied by a shifted squared sine-bell function (45−60°) and zero-filled to 4K (F_2) and 1K (F_1) data points. The influence of solvent conditions on the HCC-2 structure was addressed by increasing in a stepwise fashion the NaCl concentration in the sample up to 700 mM. All NMR data were processed and analyzed with the program package NDee (SpinUp Inc., Dortmund, Germany).

Experimental Restraints for the Structure Calculation of wt-HCC-2. NOE cross-peaks were categorized as "strong", "medium", and "weak" according to calibration against the cross-peak intensity of the δ and ϵ protons of the aromatic rings (*40*) and converted into upper limit distance constraints of 2.7, 3.3, and 5.0 Å, respectively. For distances involving either methylene protons without stereospecific assignments or methyl protons, $\langle r^{-6}\rangle^{-1/6}$ averaged distances were used (*41*). The $^3J_{HN\alpha}$ coupling constants were extracted from ω_2 cross sections of a high-resolution DQF-COSY spectrum after fitting Lorentzian lines to the antiphase doublets as described previously (*42*).

$^3J_{HN\alpha}$ values of $<$6.0 Hz were converted to ϕ angles using the Karplus equation by allowing deviations of ±20° from the derived angle, and $^3J_{HN\alpha}$ coupling constants of $>$8.0 Hz were translated to angle constraints of $-120 \pm 30°$. For the corresponding residues, a direct refinement against the J coupling constant was performed in the final stages of the calculation, allowing deviations of 1 Hz from the observed value without penalty (*43*). For non-glycine residues in which $^3J_{HN\alpha}$ was in the range of 6.0−8.0 Hz, ϕ was restrained to

be negative if the intraresidue Hα−HN NOE was less intense than the sequential Hα−HN NOE (*24*, *44*). χ^1 torsion angle restraints were determined from the two $^3J_{\alpha\beta}$ coupling constants and the intraresidue Hβ−HN NOE strength (*45*), allowing minimum ranges of ±60°. One NOE distance restraint ($d_{SS} = 2.02 \pm 0.10$ Å) was added for each of the three disulfide bonds. Hydrogen bond restraints were introduced in the final round of the calculation if three criteria were met: a slow exchange of the corresponding amide proton, a N−H···O distance of <2.3 Å, and an O···H−N angle of >120° in at least 70% of the unrestrained structures. For each hydrogen bond, two distance restraints were introduced into the calculation: $d_{HN-O} = 1.7-2.3$ Å, and $d_{N-O} = 2.4-3.3$ Å (*46*). A total of 818 experimental restraints were used for the structure calculations. Only unambiguous distance restraints were included in the initial rounds of calculation. Additional distance restraints and 39 ϕ and 14 χ^1 dihedral angle restraints were included in several rounds of structure calculation after inspection of the initial structures as described previously (*42*, *46*).

Structure Calculation and Analysis. All structures were calculated using X-PLOR 3.851 (*47*) and a modified ab initio simulated annealing protocol (*48*, *49*) which includes floating assignment of prochiral groups (*50*) and a reduced presentation for nonbonded interactions for part of the calculation (*51*). Each round of the structure calculation started from templates with random backbone torsion angles. During all stages of the simulation, the temperature was maintained by coupling to a heat bath (*52*) with a coupling frequency of 10 ps^{-1}. In the conformational search phase, 40 ps of MD was simulated at 2000 K (2 fs time step), computing nonbonded interactions only between C_α atoms and one carbon of each side chain using 2.25 Å van der Waals radii (*51*) to increase efficiency. The refinement comprised a two-phase cooling procedure treating explicitly the nonbonded interactions between all atoms. The first stage comprised cooling from 2000 to 1000 K within 30 ps (1 fs time step) and a gradual increase in the force constants for the nonbonded interactions and the angle energy constant for the diastereospecifically unassigned groups to their final values. In the next stage of the calculation, the system was cooled from 1000 to 100 K within 15 ps (1 fs time step), applying the high force constants obtained at the end of the previous cooling stage, followed by 200 steps of energy minimization.

Of the 100 structures resulting from the final round of structure calculation, those 30 structures that exhibited the lowest energy and the fewest violations of the experimental data were selected for further characterization. All calculations were carried out on Sun SparcUltra workstations requiring an average of 50 min CPU time for each calculated structure. The geometry of the structures, structural parameters, and elements of secondary structure were analyzed using the programs DSSP (*53*), PROCHECK (*54*), and PROMOTIF (*55*). For the graphical presentation of the structures, SYBYL 6.4 (Tripos Associates), MOLSCRIPT (*56*), and Raster3D (*57*) were used. The coordinates have been deposited in the Protein Data Bank (Brookhaven National Laboratory, Upton, NY) under file name 2HCC. Chemical shifts have also been deposited at the BioMagResBank (University of Wisconsin, Madison, WI) under file name 4314.

RESULTS AND DISCUSSION

Size-Exclusion Chromatography. HCC-2 eluted from a Superdex G75 column as a symmetrical peak at pH 7.4 corresponding to a molecular mass of monomeric HCC-2 (7.2 kDa). No peaks with higher elution times were observed, indicating that dimers or higher-degree oligomers are not present in solution.

Resonance Assignments and the Secondary Structure of HCC-2. Homonuclear two-dimensional NMR spectra of HCC-2 exhibit a wide dispersion of amide and C_α proton resonances from 7.14 to 9.75 ppm and from 3.36 to 5.66 ppm, respectively. Sequence-specific resonance assignments were made according to standard procedures (*58*) and allowed complete resonance assignment of all of the backbone and most of the side chain protons (available as Supporting Information). The peptide bonds of all five proline residues were in the trans-conformation as confirmed by strong NOEs between the C_δ protons of the prolines and the C_α protons of the preceding amino acid. Elements of secondary structure were identified from the intensity of the short-range NOEs, the $^3J_{HN\alpha}$ coupling constants, slow exchanging amide protons, and the chemical shift index (*59*). Helix-typical $d_{\alpha N}(i,i+3)$ and $d_{\alpha\beta}(i,i+3)$ NOEs were observed for residues 54−60 and 17−20, suggesting the presence of an α-helix and of a single helical turn. In addition, three extended strands (residues 20−25, 35−39, and 43−47) forming a triple-stranded antiparallel β-sheet were identified by the pattern of long-range NOEs and slowly exchanging amide protons. Numerous long-range NOEs indicate that the carboxy-terminal helix packs against this β-sheet (not shown; see the Supporting Information).

Tertiary Structure of HCC-2. The calculation of the final structures was based on 776 distance restraints, 53 dihedral angle restraints, and 42 hydrogen bond restraints (Table 1). The structure of HCC-2 is well-defined with backbone root-mean-square deviations (rmsds) of less than 0.35 Å for most parts of the peptide chain (Table 2). Higher backbone rmsds are found for the amino- and carboxy-terminal residues, and for the loop from residue Ser27 to Gly34. Omission of the disordered four amino-terminal and the three carboxy-terminal residues results in an overall rmsd of 0.58 and 0.96 Å for the backbone atoms and all heavy atoms, respectively (Table 2). According to PROCHECK analysis (*54*) of the family of 30 structures, all residues exhibit energetically favorable backbone conformations. Seventy-nine percent of the residues are found in the most favored regions and 21% in the allowed regions of the Ramachandran plot.

Figure 2 shows two different views of the lowest-energy structure of HCC-2 with a short α-helix and the triple-stranded antiparallel β-sheet as major elements of secondary structure. The amino terminus of the protein, whose first four residues are disordered, contains the CC motif (Cys6 and Cys7) forming disulfide bonds to Cys30 and Cys46, respectively. The stretch from Thr8 to Cys17 forms an extended series of bends and turns, which is followed by a single 3_{10}-helical turn formed by residues Cys17−Met20. This structural element is directly followed by the first β-strand (Met20−Glu25) which contains a β-bulge involving residues Ser21 and Ser22 of the first and residue Leu38 of the second β-strand. The two strands are connected by a less structured loop (Figure 1), Ser27−Gly34, which is characterized by

Table 1: Results of the Structure Calculation

experimental restraints for the final structure calculation[a]	
total no. of NOEs	776
no. of intraresidual NOEs ($\|i-j\|=0$)	313
no. of sequential NOEs ($\|i-j\|=1$)	182
no. of medium-range NOEs ($\|i-j\|=2$, 3, 4, or 5)	99
no. of long-range NOEs ($\|i-j\|>5$)	182
no. of dihedral angle restraints	53
no. of hydrogen bonds	42
molecular dynamics statistics	
average energy (kcal/mol)[b]	
E_{tot}	110.68 ± 1.90
E_{bond}	3.00 ± 0.18
E_{angle}	80.03 ± 0.92
E_{impr}	9.30 ± 0.32
E_{repel}	4.29 ± 0.62
E_{L-J}	-102.2 ± 4.35
E_{NOE}	8.29 ± 1.20
E_{cdhi}	0.01 ± 0.01
E_{coup}	5.77 ± 1.03
rmsd from ideal distances (Å)	
NOEs	0.014
bond lengths	0.002
rmsd from ideal angles (deg)	
bond angles	0.53
improper angles	0.48

[a] The number of each type of constraint is given. Each hydrogen bond is represented by two distance restraints. None of the 30 structures showed distance violations of more than 0.25 Å or dihedral angle violations of more than 2.0°. No distance or dihedral angle restraints were consistently violated by more than 0.1 Å or 1.0°, respectively. [b] E_{tot} represents the total energy, E_{repel} the repulsive energy term, and E_{NOE} the effective NOE energy term. The Lennard-Jones energy term (E_{L-J}) was not included in the target function, but was calculated using the full CHARMM potential function without further minimization.

relatively few NOE restraints. The second (Val35−Thr39) and third strand (Arg43−Ala47) are connected by a β-turn exhibiting an interesting hydrogen bonding pattern in which O_γ of Thr39 is hydrogen-bonded to the amide proton of Arg43. A loop from Lys48 to Val54 composed of two adjacent β-turns (Lys48−Gly51 and Gly51−Val54) connects the third β-strand to a regular α-helix (Val54−Lys60) that packs onto the triple-stranded antiparallel β-sheet. The presence of the third disulfide bond including Cys57 of this helix does not perturb the helical structure, as is evident in the small $^3J_{HN\alpha}$ coupling constant and the slowly exchanging amide proton of Cys57. The four carboxy-terminal residues of HCC-2 are unstructured in solution.

In addition to the disulfide bonds, the tertiary fold of the molecule is mainly stabilized by a hydrophobic core that is formed by residues from the β-sheet, the carboxy-terminal α-helix, and the extended amino terminus (Figure 3). Many of the residues involved are strictly conserved among all CC chemokines (Tyr23, Val35, Phe37, Ala47, Val54, and Leu61), suggesting that this core plays an important role in the structural integrity of the protein. Interestingly, the otherwise highly conserved Trp53 is replaced by glycine in HCC-2 (Figure 4). The same substitution has also been recognized for CKβ8 which also contains a third disulfide bond (*35*). Analysis of the structure of HCC-2 reveals that Gly53 is directly packed against the cysteines of the third disulfide bond, suggesting that a tryptophan at that position would be most probably sterically incompatible with the presence of the disulfide bond.

Comparison with Related Chemokines. The topology of the HCC-2 monomer is very similar to that of other chemokines. Both the elements of secondary structure (the triple-stranded β-sheet and the α-helix) and their spatial arrangement are highly conserved between the different CC chemokines. Even the presence of the additional disulfide bond does not lead to major structural differences between the HCC-2 topology and those of other chemokines, e.g., MIP-1β and RANTES (Figure 5).

Generally, low pairwise rmsd values are observed for the elements of regular secondary structure between different CC chemokines (Table 2). The higher values observed for the comparison to MCP-1 mainly can be attributed to the insertion of one residue in the first strand of the β-sheet in MCP-1, rendering the fitting procedure more difficult.

The rmsd values are only slightly increased after including the loop connecting the third β-strand and the α-helix in the calculation. This finding is remarkable, since in HCC-2 an otherwise strictly conserved tryptophan of this loop is replaced by glycine and the other amino acids of this loop are also only weakly conserved in HCC-2 (Figure 4).

More significant structural differences with respect to other chemokines are only observed for the amino terminus and for the loop from Ser27 to Gly34. These two regions, however, already exhibit a considerable flexibility within the family of 30 HCC-2 structures, and they were shown previously to account for the highest structural variability observed between MIP-1β and RANTES (*24*).

Many of the conserved core residues have side chain orientations in HCC-2 that are similar to those in MIP-1β, RANTES, and MCP-1. The side chain orientations are conserved not only in the core but also in the turn connecting the second and third strands of the β-sheet. Both RANTES and HCC-2 exhibit stabilization of this turn via a hydrogen bond between Thr39 O_γ and the amide proton of Arg43, resulting in a slow exchange of the amide proton of Arg43.

Despite these striking structural similarities on the level of tertiary structure with dimer-forming chemokines, HCC-2 does not form a dimeric quaternary structure under the conditions of this study. The first evidence for the monomeric structure of HCC-2 was obtained from size-exclusion chromatography, revealing an apparent molecular mass of approximately 7−8 kDa (data not shown), which is in good agreement with the calculated molecular mass of monomeric HCC-2 (7.2 kDa). This observation is confirmed by analysis of the line width in the one-dimensional NMR spectra. The peak width at half-height of the upfield-shifted methyl groups is on the order of 8−10 Hz for HCC-2, which corresponds to that of the 8 kDa monomeric protein ubiquitin. However, this value is significantly lower than the peak width at half-height of 16−18 Hz, which was reported for the dimeric chemokine RANTES (*24*).

Additional evidence for the monomeric structure of HCC-2 was deduced from the analysis of the NOE data, which is in perfect agreement with a monomeric structure as reflected by the low NOE energy term in the potential function (Table 1). None of the NOEs expected for IL-8-like or RANTES-like dimerization were observed for HCC-2. In addition, the pattern of slowly exchanging amides does not provide any evidence for dimer formation via β-sheets (not shown; see the Supporting Information).

Table 2: rmsds Resulting from Superpositions of HCC-2, RANTES, MIP-1β, and MCP-1

	rmsd (Å) of HCC-2 vs				
residues[a]	HCC-2[b] (C_α)	HCC2[b] (heavy atoms)	RANTES[c] (C_α)	MIP-1β[c] (C_α)	MCP-1[c] (C_α)
β-sheet (20−25, 35−39, and 43−47)	0.17	0.79	0.52	0.88	1.24
β-sheet and α-helix (54−60)	0.29	0.86	0.83	1.02	1.23
β-sheet, α-helix, and loop (48−53)	0.31	0.82	1.02	1.22	1.26
residues 20−63	0.57	0.99	1.31	1.49	1.50
residues 5−63	0.58	0.96	1.44	1.65	1.56

[a] Residues numbered according to the HCC-2 sequence from 1 to 66. [b] rmsd values for HCC-2 result from a best-fit superposition on the C_α atoms of the protein backbone, and were calculated by averaging the individual rmsds between the average structure and each member of the family of 30 HCC-2 structures. [c] For the comparison between HCC-2 and other chemokines, one monomeric subunit of the minimized average structure of each chemokine was used for the best-fit superposition. The PDB file names are 1RTO for RANTES, 1HUM for MIP-1β, and 1DOM for MCP-1.

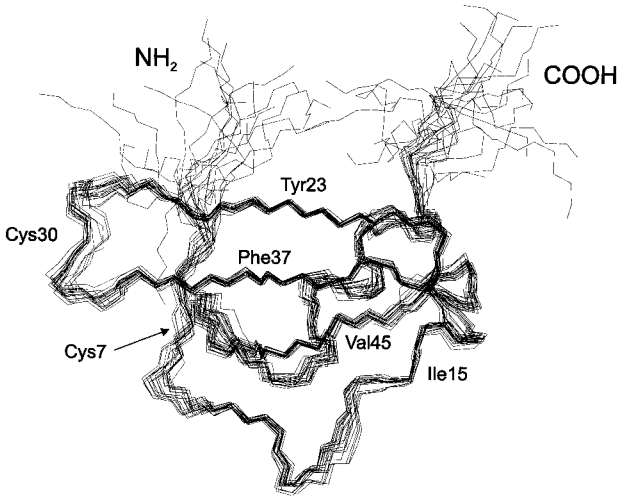

FIGURE 1: Backbone overlay of a family of 20 HCC-2 structures. The structures were included by meeting the criterion of the best energy function after the restrained molecular dynamics calculation.

Comparison of the HCC-2 structure to that of dimeric CC chemokines revealed some differences which are likely related to the monomeric structure of HCC-2. The first difference is the length of the amino terminus, which is four to six residues shorter in HCC-2 than in those chemokines that form dimers via their amino termini (Figure 4). Therefore, many of those interactions stabilizing the quaternary structure in MIP-1β, RANTES, and MCP-1 cannot be formed in HCC-2.

The role of the length of the amino terminus in the oligomerization state has been systematically addressed for MIP-1β (*60*). The results show that up to a truncation of five residues a dimeric form is favored at millimolar concentrations, while a truncation of six and more residues results in a decreased dimer affinity. After truncation of eight residues, MIP-1β exists solely as a folded monomer (*60*). These results suggest a general correlation between the length of the amino terminus and the oligomerization tendency of CC chemokines.

However, truncation of MIP-1β to an amino-terminal length that is identical to wild-type HCC-2 still results in a dimeric protein. This finding suggests that intrinsic factors such as the protein sequence or solvent conditions might play an additional role in determining the oligomerization state.

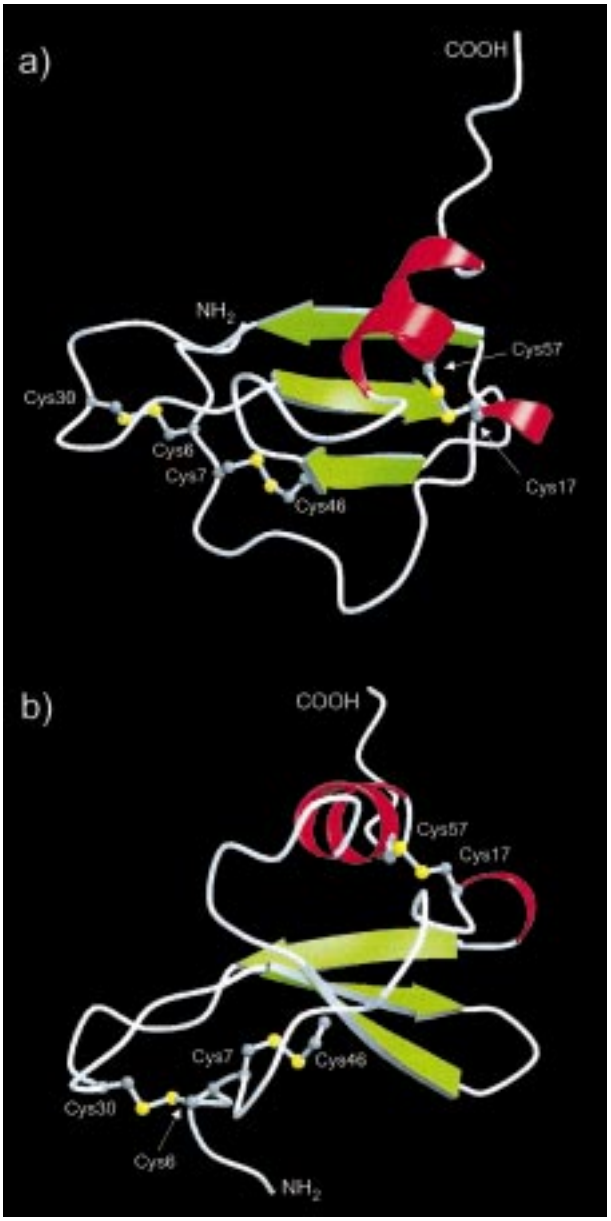

FIGURE 2: Schematic ribbon drawing indicating the elements of regular secondary structure. The cysteines forming the disulfide bonds are shown in stick representation and are labeled. The views in panels a and b are rotated 90° around the horizontal axis. This figure was drawn with MOLSCRIPT (*56*) and Raster3D (*57*).

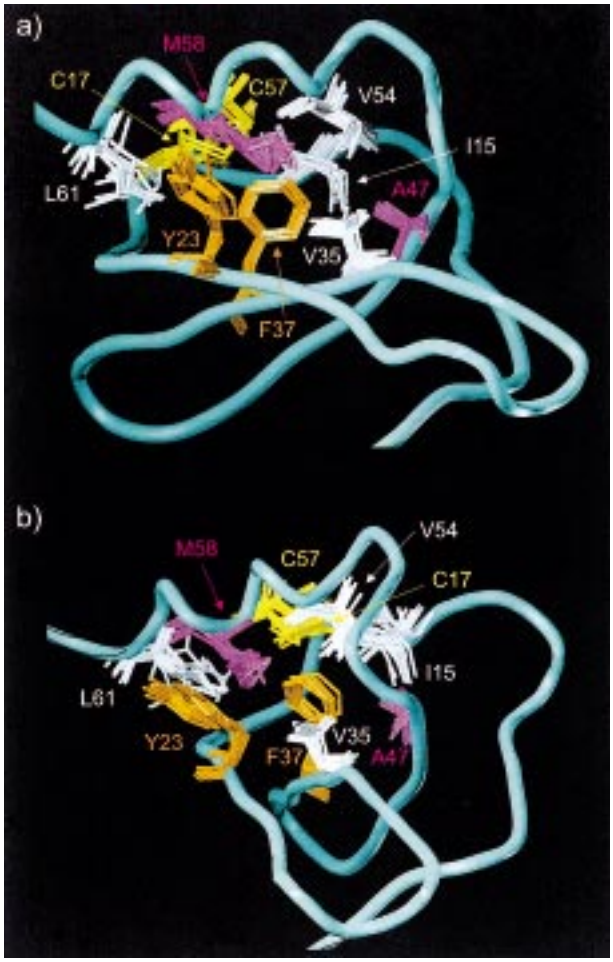

FIGURE 3: Detailed view of the region of hydrophobic interactions defining the relative orientation of the carboxy-terminal α-helix with respect to the β-sheet. Residues involved in hydrophobic contacts are shown as a best-fit superposition of the 10 lowest-energy structures. The views in panels a and b are rotated by 90° around the horizontal axis. This figure was drawn with SYBYL 6.4.

For MIP-1β, it was shown that physiological salt concentrations drastically shift the monomer−dimer equilibrium for both wild-type and most mutant proteins, favoring the dimeric form of the protein (*60*). This effect was not observed for HCC-2 in this study, and both chemical shifts and peak line widths did not change significantly after stepwise addition of sodium chloride up to a final concentration of 700 mM.

This observation strongly suggests that subtle differences in the HCC-2 sequence compared to other chemokines are responsible for the absence in dimerization affinity.

One difference is the presence of a threonine at position 8 in HCC-2. At this position, an aromatic amino acid present in all other structurally characterized CC chemokines (Figure 4) has been found previously to be part of a strongly hydrophobic stretch of amino acids that plays a role in dimerization (*61*). The corresponding residue of RANTES was shown to play a crucial role in the dimer stabilization by packing into a cavity created by residues of the other subunit (*24*).

In addition, HCC-2 contains a histidine as the first residue, while the corresponding sequence position is occupied by negatively charged (MIP-1β and RANTES) or neutral (MCP-1 and MCP-3) residues in other chemokines (Figure 4). The charged residue was found to play an important role in the formation of an intersubunit salt bridge in RANTES (Asp6−Arg47′). The presence of a histidine in HCC-2, however, renders the formation of a corresponding salt bridge electrostatically unfavorable.

The absence of charged residues and charge reversal at numerous sequence positions in HCC-2 are most probably responsible for the absence of an IL-8-like dimerization, which has also been observed in the solution structure of MCP-3 (*29*) and in one of the crystal forms of MCP-1 (*27*). In MCP-3, Tyr28 and Arg30 of the first β-strand and Asp68 of the α-helix are involved in the stabilization of the dimer (*29*). HCC-2 contains a deletion of one amino acid at the position corresponding to Arg30, and Asp68 is replaced by Lys62 in HCC-2 (Figure 4). These factors most likely contribute to the fact that the mode of dimerization reported for the MCP subfamily (*62*) is not observed in HCC-2.

The observation that HCC-2 is a monomer in a concentration range of 0.1 μM to 2 mM supports previous conclusions drawn from studies with monomeric chemokines.

For IL-8, a monomeric form of the protein has been generated by selective methylation of the amide nitrogen of Leu25, and the resulting protein had retained the structural elements present in the dimeric form (*63*). This mutant, which remains monomeric even at millimolar concentrations, was still capable of binding, attracting, and activating neutrophils (*63*).

Mutational studies with MIP-1α, which is closely related to HCC-2 in terms of sequence and function, have identified variants that are monomeric at physiological concentrations and are equipotent to the wild-type protein regarding stem cell inhibition and induction of monocyte shape change (*64*).

For the CC chemokine eotaxin, a monomer−dimer equilibrium was observed under a wide range of conditions and the structure of the monomeric form has been determined recently (*30*). In contrast to eotaxin, however, dimers could not be observed for HCC-2 under the conditions of this study.

The structure of HCC-2 confirms the assumption that for chemokine function quaternary structure is not important (*34*). This fact explains why HCC-2, which exists as a monomer over a wide range of concentrations, can also exert its physiological functions in terms of enzyme release in monocytes and eosinophil attraction (*7*). A careful comparison of HCC-2 with the structures of dimeric CC chemokines determined previously proves that the chemokine tertiary structure itself is not perturbed by quaternary contacts.

Addressing the Role of the Third Disulfide Bond. Apart from the monomeric structure, the presence of a third disulfide bond is an additional novel feature of HCC-2 compared to the chemokines that have had their structures determined so far. As this disulfide bond does not induce significant structural differences with respect to MIP-1β and RANTES, this raises the question about the role of the disulfide bond in the structure of HCC-2.

One hypothesis was that this disulfide bond might play a role in defining the orientation of the helix relative to the β-sheet. We addressed this question by investigating the structure of a HCC-2 mutant in which the two cysteines forming the additional disulfide bond were replaced by alanine. Evaluation of the NOE data for this mutant revealed

```
                    1        10        20        30        40        50        60
                    |        |         |         |         |         |         |
HCC-2       ------HFAADCCTSYISQSIPCSLMKSY-FETSSECSKPGVIFLTKKGRQVCAKPSGPGVQDCMKKLKPYSI----
MIP-1ß      -APMGSDPPTACCFSYTARKLPRNFVVDY-YETSSLCSQPAVVFQTKRSKQVCADPSESWVQEYVYDLELN------
RANTES      -SPYSSDT-TPCCFAYIARPLPRAHIKEY-FYTSGKCSNPAVVFVTRKNRQVCANPEKKWVREYINSLEMS------
MCP-1       MQPDAINAPVTCCYNFTNRKISVQRLASYRRITSSKCPKEAVIFKTIVAKEICADPKQKWVQDSMDHLDKQ------
MCP-3       -QPVGINTSTTCCYRFINKKIPKQRLESYRRTTSSHCPREAVIFKTKLDKEICADPTQKWVQDFMKHLDKKTQTPKL
EOTAXIN     ---GPASVPTTCCFNLANRKIPLQRLESYRRITSGKCPQKAVIFKTKLAKDICADPKKKWVQDSMKYLDQKSPTPKP
                         **     . .    .  *   **  *    *.* *   . .** *    *.. .  *
```

FIGURE 4: Sequence alignment between the six CC chemokines, for which high-resolution structures are available (ClustalW; *65*). Strictly conserved residues are denoted with an asterisk, and positions with conservative substitutions are denoted with a dot. The amino acid numbering is given according to the HCC-2 sequence of 66 residues.

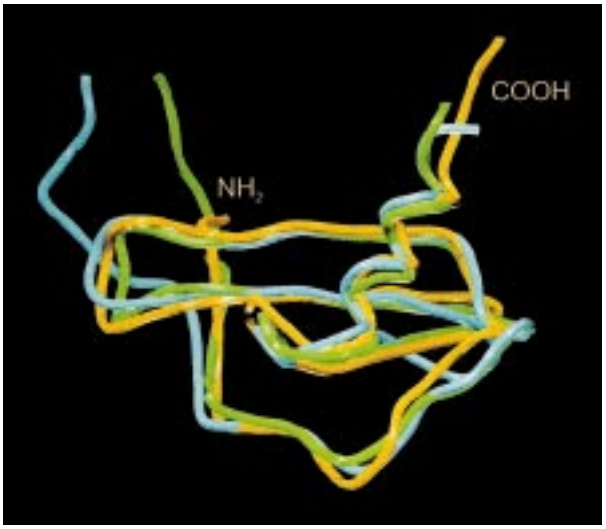

FIGURE 5: Backbone overlay of HCC-2 (yellow), RANTES (blue), and MIP-1β (green) in tube representation.

that all contacts observed between the helix and the sheet in wild-type HCC-2 are still present in the mutant. The pattern and intensity of the NOEs are similar in the mutant, as shown in Figure 6 for the interaction between the aromatic ring of Tyr23 and the side chain of Met58. It appears that the relative orientation of the helix toward the sheet does not depend on the presence or absence of this additional disulfide bond.

The only residue in HCC-2, which is affected by the Cys to Ala replacement, is Ile15. The NOE pattern of this residue is largely unchanged, but the shifts of the side chain proton resonances change by up to 0.3 ppm in the mutant, indicating subtle changes of the side chain orientation. The close proximity of Phe37 to Ile15 (Figure 3) gives rise to ring current effects, thus rendering chemical shifts a very sensitive indicator for monitoring structural changes. Therefore, one might speculate that the additional disulfide bond mainly plays a role in stabilizing the orientation of amino-terminal residues 15−20.

This proposed role of the disulfide bond is also in agreement with the fact that the loop formed by the residues of positions 15−20 is stabilized by Trp53 in other chemokines (*26*). The lack of this tryptophan might therefore be compensated by the presence of the disulfide bond in HCC-2. These findings suggest that a tryptophan is not necessary for determining the orientation of the helix relative to the β-sheet but plays a role in stabilizing the helical turn formed by amino acids 17−20, a role that might be compensated by the disulfide bond in HCC-2.

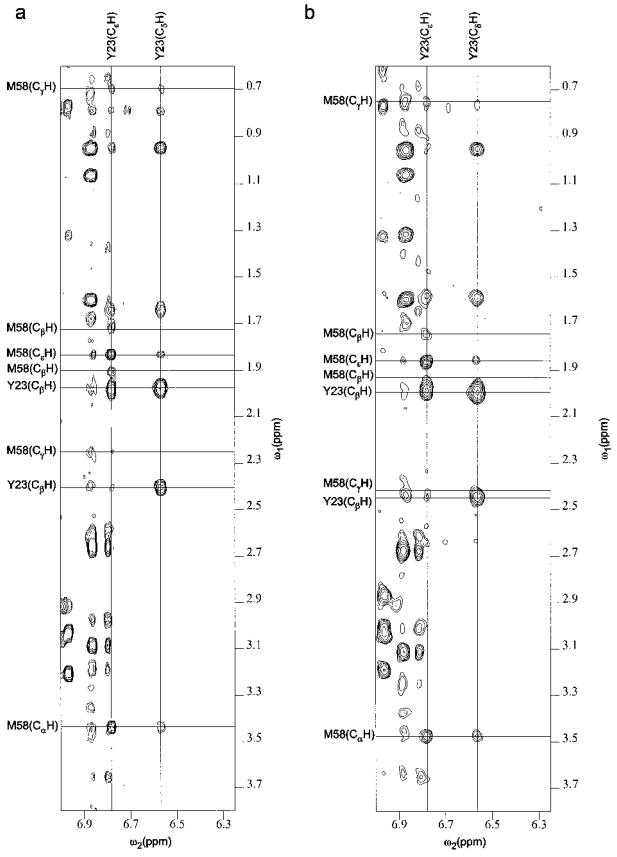

FIGURE 6: Comparison of the helix orientation between (a) wt-HCC-2 and (b) the mutant [Ala[17,57]]HCC-2. All NOEs between the aromatic ring of Tyr23 and the side chain of Met58 are shown.

SUPPORTING INFORMATION AVAILABLE

A table containing the ^{1}H chemical shifts of wt-HCC-2 at 25 °C and pH 3.0 and four figures showing the fingerprint region of a TOCSY spectrum, the secondary structure of HCC-2, the spatial interactions of the different amino acids, and the distribution of NOEs, respectively. This material is available free of charge via the Internet at http://pubs.acs.org.

REFERENCES

1. Taub, D. (1996) *Cytokine Growth Factor Rev. 7*, 355−376.
2. Moser, B., Loetscher, M., Piali, L., and Loetscher, P. (1998) *Int. Rev. Immunol. 16*, 323−344.
3. Baggiolini, M., Dewald, B., and Moser, B. (1997) *Annu. Rev. Immunol. 15*, 675−705.
4. Baggiolini, M., Loetscher, P., and Moser, B. (1995) *Int. J. Immunopharmacol. 17*, 103−108.
5. Lusti-Narasimhan, M., Chollet, A. C., Power, C. A., Allet, B., Proudfoot, A. E. I., and Wells, T. N. C. (1996) *J. Biol. Chem. 271*, 3148−3153.

6. Murphy, P. M. (1994) *Annu. Rev. Immunol. 12*, 593−633.
7. Pardigol, A., Forssmann, U., Zucht, H. D., Loetscher, P., Schulz-Knappe, P., Baggiolini, M., Forssmann, W. G., and Mägert, H. J. (1998) *Proc. Natl. Acad. Sci. U.S.A. 95*, 6308−6313.
8. Youn, B. S., Zhang, S. M., Lee, E. K., Park, D. H., Broxmeyer, H. E., Murphy, P. M., Locati, M., Pease, J. E., Kim, K. K., Antol, K., and Kwon, B. S. (1997) *J. Immunol. 159*, 5201−5205.
9. Coulin, F., Power, C. A., Alouani, S., Peitsch, M. C., Schroeder, J. M., Moshizuki, M., Clark-Lewis, I., and Wells, T. N. C. (1997) *Eur. J. Biochem. 248*, 507−515.
10. St. Charles, R., Walz, D. A., and Edwards, B. F. (1989) *J. Biol. Chem. 264*, 2092−2099.
11. Zhang, X., Chen, L., Bancroft, D. P., Lai, C. K., and Maione, T. E. (1994) *Biochemistry 33*, 8361−8366.
12. Clore, G. M., Appella, E., Yamada, M., Matsushima, K., and Gronenborn, A. M. (1990) *Biochemistry 29*, 1689−1696.
13. Baldwin, E. T., Weber, I. T., St. Charles, R., Xuan, J. C., Appella, E., Yamada, M., Matsushima, K., Edwards, B. F., Clore, G. M., Gronenborn, A. M., and Wlodawer, A. (1991) *Proc. Natl. Acad. Sci. U.S.A. 88*, 502−506.
14. Fairbrother, W. J., Reilly, D., Colby, T., and Horuk, R. (1993) *FEBS Lett. 330*, 302−306.
15. Fairbrother, W. J., Reilly, D., Colby, T. J., Hesselgesser, J., and Horuk, R. (1994) *J. Mol. Biol. 242*, 252−270.
16. Kim, K. S., Clark-Lewis, I., and Sykes, B. D. (1994) *J. Biol. Chem. 269*, 32909−32915.
17. Sticht, H., Auer, M., Schmitt, B., Besemer, J., Horcher, M., Kirsch, T., Lindley, I. J. D., and Rösch, P. (1996) *Eur. J. Biochem. 235*, 26−35.
18. Hanzawa, H., Haruyama, H., Konishi, K., Watanabe, K., and Tsurufuji, S. (1998) *J. Biochem. 123*, 62−70.
19. Hanzawa, H., Haruyama, H., Watanabe, K., and Tsurufuji, S. (1994) *FEBS Lett. 354*, 207−212.
20. Malkowski, M. G., Wu, J. Y., Lazar, J. B., Johnson, P. H., and Edwards, B. F. (1995) *J. Biol. Chem. 270*, 7077−7087.
21. Shao, W., Jerva, L. F., West, J., Lolis, E., and Schweitzer, B. I. (1998) *Biochemistry 37*, 8303−8313.
22. Dealwis, C., Fernandez, E. J., Thompson, D. A., Simon, R. J., Siani, M. A., and Lolis, E. (1998) *Proc. Natl. Acad. Sci. U.S.A. 95*, 6941−6946.
23. Lodi, P. J., Garrett, D. S., Kuszewski, J., Tsang, M. L.-S., Weatherbee, J. A., Leonard, W. J., Gronenborn, A. M., and Clore, G. M. (1994) *Science 263*, 1762−1767.
24. Skelton, N. J., Aspiras, F., Ogez, J., and Schall, T. J. (1995) *Biochemistry 34*, 5329−5342.
25. Chung, C. W., Cooke, R., Proudfoot, A. E. I., and Wells, T. N. C. (1995) *Biochemistry 34*, 9307−9314.
26. Handel, T. M., and Domaille, P. J. (1996) *Biochemistry 35*, 6569−6584.
27. Lubkowski, J., Bujacz, G., Boqué, L., Domaille, P. J., Handel, T. M., and Wlodawer, A. (1997) *Nat. Struct. Biol. 4*, 64−69.
28. Kim, K. S., Rajarathnam, K., Clark-Lewis, I., and Sykes, B. D. (1996) *FEBS Lett. 395*, 277−282.
29. Meunier, S., Bernassau, J. M., Guillemot, J. C., Ferrara, P., and Darbon, H. (1997) *Biochemistry 36*, 4412−4422.
30. Crump, M. P., Rajarathnam, K., Kim, K.-S., Clark-Lewis, I., and Sykes, B. D. (1998) *J. Biol. Chem. 273*, 22471−22479.
31. Tanaka, Y., Adams, D. H., Hubscher, S., Hirano, H., Siebenlist, U., and Shaw, S. (1993) *Nature 361*, 79−82.
32. Burrows, S. D., Doyle, M. L., Murphy, K. P., Franklin, S. G., White, J. R., Brooks, I., McNulty, D. E., Scott, M. O., Knutson, J. R., Porter, D., Young, P. R., and Hensley, P. (1994) *Biochemistry 33*, 12741−12745.
33. Paolini, J. F., Willard, D., Consler, T., Luther, M., and Krangel, M. S. (1994) *J. Immunol. 153*, 2704−2717.
34. Clark-Lewis, I., Kim, K. S., Rajarathnam, K., Gong, J. H., Dewald, B., Moser, B., Baggiolini, M., and Sykes, B. D. (1995) *J. Leukocyte Biol. 57*, 703−711.
35. Forssmann, U., Belen Degado, M., Uguccioni, M., Loetscher, P., Garotta, G., and Baggiolini, M. (1997) *FEBS Lett. 408*, 211−216.
36. Cavanagh, J., and Rance, M. (1992) *J. Magn. Reson. 96*, 670−678.
37. Marion, D., Ikura, M., Tschudin, R., and Bax, A. (1989) *J. Magn. Reson. 85*, 393−399.
38. Hwang, T.-L., and Shaka, A. J. (1995) *J. Magn. Reson. 112A*, 275−279.
39. van Zijl, P. C. M., O'Neill Johnson, M., Mori, S., and Hurd, R. E. (1995) *J. Magn. Reson. 113A*, 265−270.
40. Eberle, W., Pastore, A., Sander, C., and Rösch, P. (1991) *J. Biomol. NMR 1*, 71−82.
41. Clore, G. M., Gronenborn, A. M., Nilges, M., and Ryan, C. A. (1987) *Biochemistry 26*, 8012−8023.
42. Beissinger, M., Sticht, H., Sutter, M., Ejchart, A., Haehnel, W., and Rösch, P. (1998) *EMBO J. 17*, 27−36.
43. Garrett, D. S., Kuszewski, J., Hancock, T. J., Lodi, P. J., Vuister, G. W., Gronenborn, A. M., and Clore, G. M. (1994) *J. Magn. Reson. B104*, 99−103.
44. Clubb, R. T., Ferguson, S. B., Walsh, C. T., and Wagner, G. (1994) *Biochemistry 33*, 2761−2772.
45. Wagner, G., Braun, W., Havel, T. F., Schaumann, T., Go, N., and Wüthrich, K. (1987) *J. Mol. Biol. 196*, 611−639.
46. Kraulis, P. J., Clore, G. M., Nilges, M., Jones, T. A., Petterson, G., Knowles, J., and Gronenborn, A. M. (1989) *Biochemistry 28*, 7241−7257.
47. Brünger, A. T. (1993) *X-PLOR*, version 3.1, Howard Hughes Medical Institute and Yale University, New Haven, CT.
48. Kharrat, A., Macias, M. J., Gibson, T. J., Nilges, M., and Pastore, A. (1995) *EMBO J. 14*, 3572−3584.
49. Kemmink, J., Darby, N. J., Dijkstra, K., Nilges, M., and Creighton, T. E. (1996) *Biochemistry 35*, 7684−7691.
50. Holak, T. A., Nilges, M., and Oschkinat, H. (1989) *FEBS Lett. 242*, 649−654.
51. Nilges, M. (1993) *Proteins 17*, 297−309.
52. Berendsen, H. J. C., Postma, J. P. M., van Gunsteren, W. F., DiNiola, A., and Haak, J. R. (1984) *J. Chem. Phys. 81*, 3684−3690.
53. Kabsch, W., and Sander, C. (1983) *Biopolymers 22*, 2577−2637.
54. Laskowski, R. A., MacArthur, M. W., Moss, D. S., and Thornton, J. M. (1993) *J. Appl. Crystallogr. 26*, 283−291.
55. Hutchinson, E. G., and Thornton, J. M. (1996) *Protein Sci. 5*, 212−220.
56. Kraulis, P. (1991) *J. Appl. Crystallogr. 24*, 946−950.
57. Merritt, E. A., and Murphy, M. E. P. (1994) *Acta Crystallogr. D50*, 869−873.
58. Wüthrich, K. (1986) *NMR of proteins and nucleic acids*, John Wiley and Sons, New York.
59. Wishart, D. S., Bigam, C. G., Holm, A., Hodges, R. S., and Sykes, B. D. (1995) *J. Biomol. NMR 5*, 67−81.
60. Laurence, J. S., LiWang, A. C., and LiWang, P. J. (1998) *Biochemistry 37*, 9346−9354.
61. Covell, D. G., Smythers, G. W., Gronenborn, A. M., and Clore, G. M. (1994) *Protein Sci. 3*, 2064−2072.
62. Proost, P., Wuyts, A., and Van Damme, J. (1996) *J. Leukocyte Biol. 59*, 67−74.
63. Rajarathnam, K., Sykes, B. D., Kay, C. M., Dewald, B., Geiser, T., Baggiolini, M., and Clark-Lewis, I. (1994) *Science 264*, 90−92.
64. Graham, G. J., MacKenzie, J., Lowe, S., Tsang, M. L., Weatherbee, J. A., Issacson, A., Medicherla, J., Fang, F., Wilkinson, P. C., and Pragnell, I. B. (1994) *J. Biol. Chem. 269*, 4974−4978.
65. Higgins, D. G., Bleasby, A. J., and Fuchs, R. (1992) *Comput. Appl. Biosci. 8*, 189−191.

BI990065I